JOURNAL OF GEOPHYSICAL RESEARCH, VOL. 114, A12211, doi:10.1029/2009JA014614, 2009

Ion distributions near the reconnection sites: Comparison between simulations and THEMIS observations

X.-Z. Zhou,[1] V. Angelopoulos,[1] A. Runov,[1] M. I. Sitnov,[2] Q.-G. Zong,[3,4] and Z. Y. Pu[3]

Received 29 June 2009; revised 1 August 2009; accepted 26 August 2009; published 16 December 2009.

[1] We study the evolution of ion distribution functions in a magnetotail thin current sheet using as a case study the 26 February 2008 substorm event observed by the THEMIS mission. The observed mushroom-shaped velocity space ion distributions, whereby warmer ions are mostly moving duskward, are shown to appear when the current sheet thickness becomes comparable with thermal ion gyroradius. As magnetic reconnection starts earthward of the THEMIS satellite (probe) P1, these duskward moving warmer ions also start to stream tailward, gradually separating in velocity space from the colder ions that dominate the density moment. Test particle simulations demonstrate that the observed evolution of ion distributions is consistent with cucumber-type trajectories in a current sheet with an X-type configuration.

Citation: Zhou, X.-Z., V. Angelopoulos, A. Runov, M. I. Sitnov, Q.-G. Zong, and Z. Y. Pu (2009), Ion distributions near the reconnection sites: Comparison between simulations and THEMIS observations, *J. Geophys. Res.*, *114*, A12211, doi:10.1029/2009JA014614.

1. Introduction

[2] During the late growth phase of geomagnetic substorms, one of the most significant signatures in the near-Earth magnetotail is the formation of thin current sheets (TCSs) [e.g., *Baumjohann et al.*, 2007, and references therein]. The current sheet thickness can become as small as several hundred kilometers [e.g., *Sergeev et al.*, 1993; *Asano et al.*, 2004; *Runov et al.*, 2008], that is, on the order of the thermal ion gyroradius.

[3] In the TCSs the minimum curvature radius of the magnetic field is usually smaller than the thermal ion gyroradius (with the curvature parameter κ defined by *Büchner and Zelenyi* [1989] as less than unity), which suggests that the ions could be unmagnetized, and thus their orbits could deviate significantly from the conventional Larmor gyrations. *Speiser* [1965] first suggested that particles could meander across the neutral sheet before they were eventually ejected from the current sheet. In addition to the well-known Speiser-type transient orbits, two classes of trapped orbits, i.e., the ring-type trajectories and the cucumber-type ones, have been theoretically identified [*Büchner and Zelenyi*, 1989]. The ring-type trajectories are characterized by fast oscillations in the z direction (the direction normal to the current sheet) with the particle moving across the neutral sheet periodically and by slower circular motions in the xy plane (the tangent plane of the current sheet). The cucumber-type trajectories, on the other hand, differ from the ring-type ones in that the particle motion can be divided into a neutral sheet-crossing segment and a noncrossing one during each particle circle in the xy plane.

[4] Furthermore, a new adiabatic invariant, that is, the sheet invariant I_z [e.g., *Sonnerup*, 1971; *Büchner and Zelenyi*, 1989; *Ashour-Abdalla et al.*, 1993; *Zhou et al.*, 2007], has been introduced in current sheets with $\kappa \ll 1$ to replace the traditional invariants. It has been shown that the ions following ring-type trajectories would be adiabatic with respect to I_z, and those cucumber-type ions would become quasi-adiabatic [*Büchner and Zelenyi*, 1989] with a scattering of I_z at the transition region between the neutral sheet-crossing and the noncrossing segments.

[5] Information regarding the particle dynamics in the TCSs could be provided by the observations of particle velocity distribution functions. It has been suggested by *Hoshino et al.* [1998] that anisotropic and nongyrotropic ion distributions often observed in the TCSs might be kinetic signatures of magnetic reconnection arising from the plasma mixing between the meandering ions accelerated around the X-type region and the cold ions convected directly from the lobe. To better understand the effect of the X-type configuration on particle dynamics and distributions, both test particle simulations [e.g., *Martin and Speiser*, 1988; *Speiser and Martin*, 1992; *Büchner and Kuska*, 1998], under prescribed electric and magnetic fields, and hybrid simulations [e.g., *Nakamura et al.*, 1998; *Lottermoser et al.*, 1998], with ions being treated as particles under charge-neutralizing electron fluid, have been carried out, which

[1]Institute of Geophysics and Planetary Physics, University of California, Los Angeles, California, USA.
[2]Johns Hopkins University Applied Physics Laboratory, Laurel, Maryland, USA.
[3]School of Earth and Space Sciences, Peking University, Beijing, China.
[4]Also at Center for Atmospheric Research, University of Massachusetts Lowell, Lowell, Massachusetts, USA.

0148-0227/09/2009JA014614$09.00

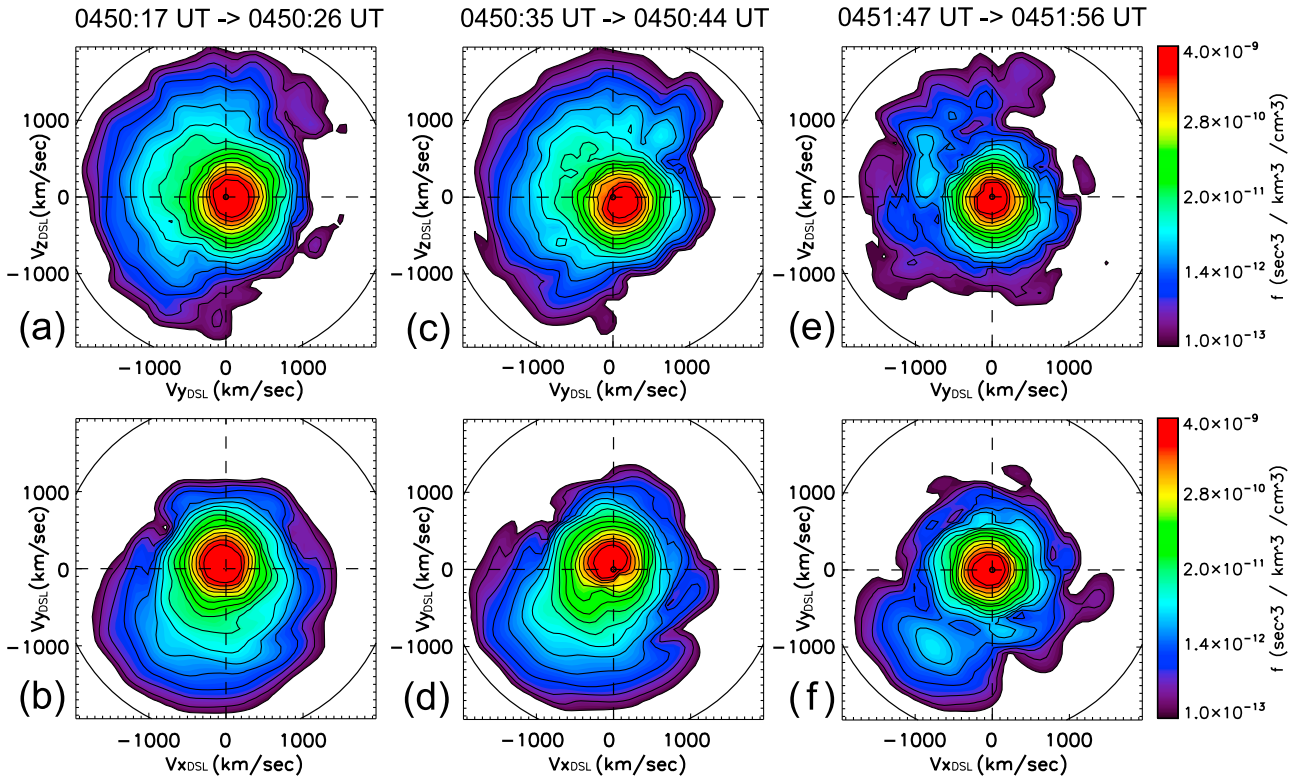

Figure 1. THEMIS P1 observations of the ion distribution functions in despun spacecraft coordinates (+*x* is earthward, +*y* is dawnward, and +*z* is southward) during the substorm event of 26 February 2008. (a and b) Cuts of the three-dimensional ion velocity distribution in the *yz* and the *xy* plane, respectively, observed during 0450:17–0450:26 UT. (c and d) Cuts of the distribution in *yz* and *xy* observed during 0450:35–0450:44 UT. (e and f) Cuts of the distribution in *yz* and *xy* observed during 0451:47–0451:56 UT.

makes certain predictions on the shapes of particle distribution functions during reconnection, for example, the ridge structures and the partial shell structures in the ion distribution functions.

[6] With the recent availability of high-quality, high time resolution three-dimensional particle distributions from numerous crossings of the tail current sheet by the THEMIS mission [*Angelopoulos*, 2008], it is now possible to understand the magnetotail particle dynamics in depth by directly comparing particle orbit simulation results with observations. In this paper, we study the evolution of the ion distributions observed by the THEMIS satellite (probe) P1 (or THEMIS-B) in the TCS tailward of the reconnection site during the substorm event of 26 February 2008. As the overview of this substorm event has been given by *Angelopoulos et al.* [2008] and *Pu et al.* [2009], the current sheet profiles and the associated particle distribution functions were self-consistently modeled by *Zhou et al.* [2009] to explain the observed duskward anisotropy in the ion distributions during the late growth phase of this particular substorm event, in the absence of a magnetic field component normal to the current sheet (B_z). The *Zhou et al.* [2009] modeling could not, however, reproduce the tailward anisotropy observed right after the southward turning of the magnetic field. Here we use test particle simulations in prescribed fields to explain these observed features of the ion distributions. We show that the tailward anisotropy can be naturally explained as the result of an X-type configuration that results in cucumber-type trajectories in the reconnecting current sheet.

2. Observations

[7] In this study, the THEMIS data from the electrostatic analyzer instrument [*McFadden et al.*, 2008], the fluxgate magnetometer instrument [*Auster et al.*, 2008], and the electric field instrument [*Bonnell et al.*, 2008] are used. Figure 1 shows the time evolution of the ion distributions observed by THEMIS P1 (TH-B) during the 26 February 2008 substorm event in despun spacecraft coordinates (+*x* is earthward, +*y* is dawnward, and +*z* is southward, which is opposite to the GSM coordinate in the *y* and *z* directions). Figures 1a, 1c, and 1e show cuts of the ion distribution in the *yz* plane during the time intervals indicated, while Figures 1b, 1d, and 1f correspond to cuts in the *xy* plane. It should be noted that probe P1 was located close to the southern edge of the thin current sheet with the observed magnetic field predominantly in the −*x* direction, implying that the *yz* cuts shown in Figures 1a, 1c, and 1e are the distributions in the plane perpendicular to the magnetic field. To reduce statistical fluctuations with minimal loss of time resolution the distributions are averaged over three spin periods (9 s).

[8] Figures 1a and 1b correspond to the time interval of 0450:17–0450:26 UT, which is within the late growth phase of the substorm. As was suggested by *Zhou et al.*

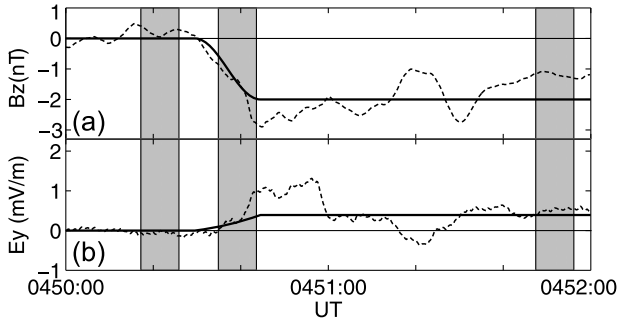

Figure 2. The P1 observations of (a) the magnetic field B_z component and (b) the 3 s sliding averaged electric field E_y component in the GSM coordinate system, shown as the dashed lines. Also shown as the solid lines are the adopted B_z and E_y fields at the P1 location, which are superposed to the modeled thin current sheet fields [*Zhou et al.*, 2009] to be used in the test particle simulations to model the time evolution of the ion distributions. The three time intervals shown in Figures 1 and 3 are highlighted as shaded areas here.

[2009], the observed ions could be separated into a colder (~500 eV) and a warmer (~10 keV) component, and the most pronounced feature of the ion distribution is the strong anisotropy and nongyrotropy of the warmer component with a higher flux of duskward moving ions than those moving dawnward. These nongyrotropic warmer ions, along with the quasi-isotropic colder ones, compose a mushroom-shaped structure in the *yz* plane shown in Figure 1a. The ion distribution in the *xy* plane, on the other hand, is essentially symmetric with respect to the *y* axis (see Figure 1b).

[9] At onset of magnetic reconnection, P1 was located in the current sheet tailward of the reconnection site [*Angelopoulos et al.*, 2008] observing a southward turning of the B_z field at 0450:30 UT, which is shown in Figure 2a with a dashed line (in GSM coordinates). It is interesting to note that the observed ion distributions (shown in Figures 1c–1f) also evolved in time as the magnetic field turned southward.

[10] Figures 1c and 1d suggest the *yz* and *xy* cuts of the ion distribution during 0450:35–0450:44 UT, which is 5–14 s after the southward turning of the magnetic field. The distribution of colder ions shows very small changes, and the mushroom-shaped structure in the *yz* plane also remains; however, the previous symmetry in the *xy* plane (shown in Figure 1b) with respect to the *y* axis disappears in Figure 1d, with the duskward moving warmer ions also starting to experience tailward motions.

[11] The phase space density for the warmer ion component gradually decreases as reconnection continues, which could be seen in Figures 1e and 1f as the *yz* and *xy* cuts of the ion distribution during 0451:47–0451:56 UT. More interestingly, the ion distribution becomes double peaked with the warmer ion component streaming duskward and tailward, well separated from the colder one by a gap between them.

3. Simulations and Interpretations

[12] As was suggested by *Zhou et al.* [2009], the observed ion distribution before the southward turning of the magnetic field could be modeled by a modified Sitnov-Guzdar-Swisdak (SGS) equilibrium [*Sitnov et al.*, 2003, 2004, 2006], which assumes the particle distributions can be taken as functions of three invariants of motion (the particle energy W, the y component of the canonical momentum P_y, and the sheet invariant I_z) to automatically satisfy the Vlasov equation. The assumed particle distributions $f(W, P_y, I_z)$ are then substituted into the Maxwell equations to self-consistently obtain the solution of particle distributions $f(\mathbf{r}, \mathbf{v})$ within the entire thin current sheet, along with the current sheet profiles of the magnetic and electric fields and the relative location of probe P1 within the current sheet.

[13] Figures 3a and 3b show the *yz* and *xy* cuts of the modeled ion distribution at the P1 location, i.e., 1260 km south of the neutral sheet [*Zhou et al.*, 2009]. It can be clearly seen that the modified SGS equilibrium can reproduce most of the key features of the P1 observations shown in Figures 1a and 1b, i.e., the anisotropic and nongyrotropic warmer ion component and the mushroom-shaped structure in the *yz* plane, which could be understood as the combined effect of the diamagnetic drift and the coexistence of meandering and gyrating ions in the TCS. Note that the duskward moving warmer ions are mostly experiencing meandering motions across the neutral sheet [*Zhou et al.*, 2009].

[14] After the southward turning of the magnetic field at 0450:30 UT the modified SGS equilibrium can no longer reproduce the observed ion distributions within the current sheet. However, the particle distributions within the modeled equilibrium can still be treated as the initial condition to be associated with the particle distributions at later time intervals, on the basis of Liouville's theorem [e.g., *Schwartz et al.*, 1998] that the phase space density is constant along particle trajectories, i.e., $f(\mathbf{r}, \mathbf{v}, t) = f_0(\mathbf{r}_0, \mathbf{v}_0, t_0)$. In other words, the ion distributions f at later time intervals may be achieved by tracing the ion trajectories backward in time to obtain the ion locations and velocities within the initial equilibrium at t_0 = 0450:30 UT and equating the current phase space density $f(\mathbf{r}, \mathbf{v}, t)$ with the corresponding $f_0(\mathbf{r}_0, \mathbf{v}_0, t_0)$ values.

[15] Our simulation model to display the time evolution of the ion distributions is then constructed on the basis of the computation of ion trajectories in the modeled thin current sheet by applying a fourth-order Runge-Kutta scheme with corrections at each step to ensure energy conservation. The magnetic and electric fields adopted in the simulation model are assumed to be the same as the fields modeled in the initial equilibrium, shown by *Zhou et al.* [2009, Figure 5a], except for a superposition of a GSM B_z component (unit in nanotesla):

$$B_z(x,t) = \left[1 - \cos\frac{(t-t_0)\pi}{15}\right] \cdot (x + 18.5)/3 \qquad 0 \le t - t_0 < 15$$

$$B_z(x,t) = 2(x + 18.5)/3 \qquad t - t_0 \ge 15$$

to model the development of the X-type configuration. Here the location (unit in R_E) of the reconnection site is assumed to be $x = -18.5$, which is 3 R_E earthward of the probe P1 and is consistent with the conclusion made by *Angelopoulos et al.* [2008] that reconnection occurred somewhere between probes P1 ($x = -21.5$) and P2 ($x = -17.1$). Note that the

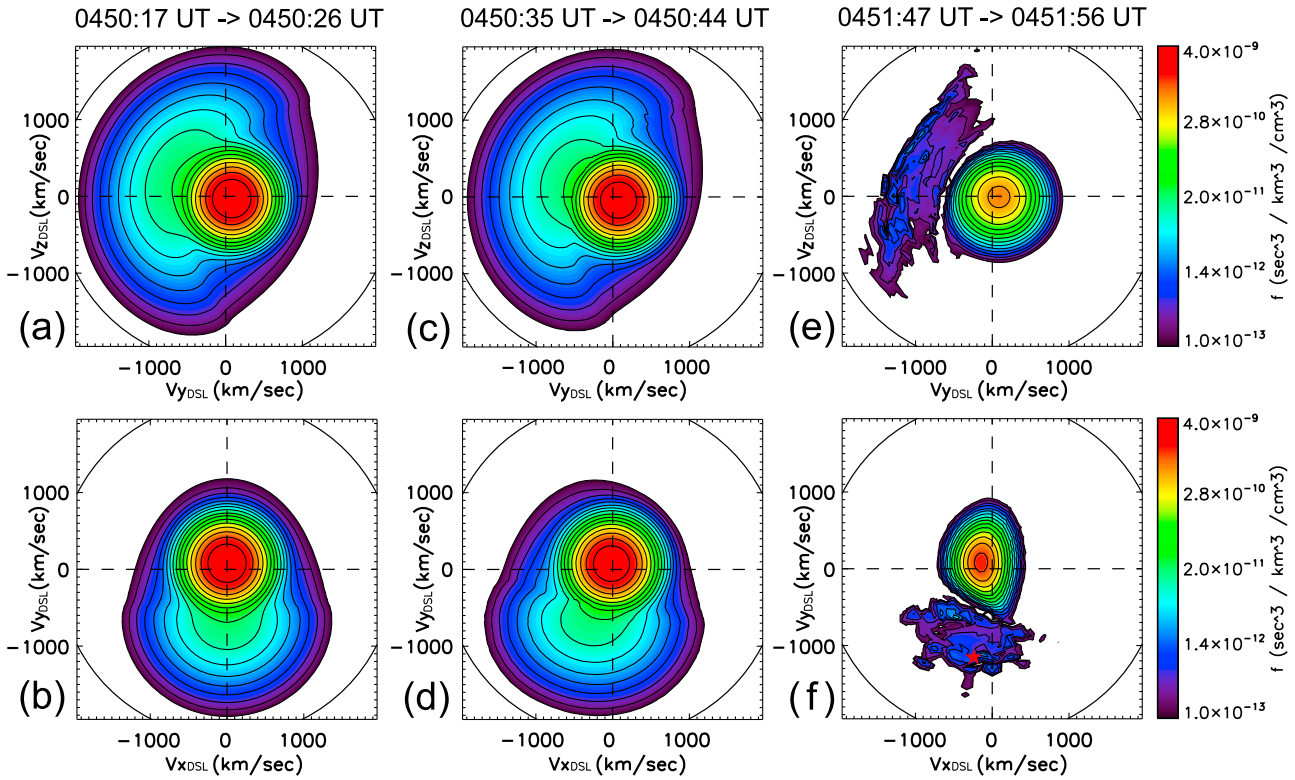

Figure 3. Same format as Figure 1 but displaying the evolution of the simulated ion distribution functions at the spacecraft location during different time intervals. The red star in Figure 3f corresponds to the final velocity of the ion trajectory shown in Figure 4.

southward B_z field equals −2.0 nT at the P1 location, which corresponds to the minimum radius curvature of ∼100 km. The gyroperiod of thermal ions moving at the velocity of ∼300 km/s, on the other hand, is ∼2000 km, suggesting a κ value of ∼0.22 well below unity to satisfy the *Büchner and Zelenyi* [1989] theory. Also superposed in the model is a dawn-dusk electric field E_y (unit in mV/m):

$$E_y(x,t) = 0.024(t-t_0) - \frac{\pi(x+18.5)^2}{573.4}\sin\frac{\pi(t-t_0)}{15} \qquad 0 \le t-t_0 < 15$$
$$E_y(x,t) = 0.36 \qquad t-t_0 \ge 15,$$

which is built up in accordance with Faraday's law to model the electric field associated with the reconnection process from 0 during the initial equilibrium to the final value of 0.36 mV/m. It should be noted that the dawn-dusk electric field could not be Lorentz transformed away by simply assuming a uniform deHoffman-Teller frame, like what has been done in some previous studies [e.g., *Speiser*, 1965], because of the time and location dependence of the E_y and B_z fields. However, the convection velocity $v_c(x, t) = E_y(x, t)/B_z(x, t)$ in the x direction could still be treated as the local deHoffman-Teller velocity to the lowest-order approximation [*Ashour-Abdalla et al.*, 1993; *Drake et al.*, 2009].

[16] The time-dependent B_z and E_y fields used in the simulation model, at the P1 location, are shown as the solid lines in Figures 2a and 2b, respectively. The adopted fields could be treated as a reasonable simplification of the observed B_z and E_y fields (shown as the dashed lines) to avoid obscuring the underlying physics. It should be noted that the instantaneous local magnetic and electric fields during magnetic reconnection could be much more complicated than those adopted in our simulation, and we do not attempt here to obtain an accurate model of reconnection in a self-consistent manner, but our approach may be justified by the fact that particle orbits scan a large region of space and respond to large-scale averages of the fields for which long-term time averages may be a valid approximation. It should be also noted that the initial equilibrium suggests that the particle distributions be independent of x and y values at t_0, which could be another error source as there must be a spatial limit beyond which the modified SGS solution of the thin current sheet is not accurate. However, even the simplified model used in our simulations results in a time evolution of the simulated ion distributions shown in Figure 3 that adequately reproduces the observed features shown in Figure 1.

[17] Figures 3c and 3d present the simulation result of the 9-s-averaged ion distribution in the yz and the xy planes, respectively, at the P1 location during 0450:35–0450:44 UT (5–14 s later than the magnetic field southward turning). The time evolution of the simulated ion distributions is shown to be very similar to the evolution of the observed ones; for example, the mushroom-shaped structure in the initial equilibrium remains in the yz plane, and the ions initially meandering duskward also start to move tailward.

[18] The additional tailward motions of the ions initially following meandering orbits could be understood as Speiser-

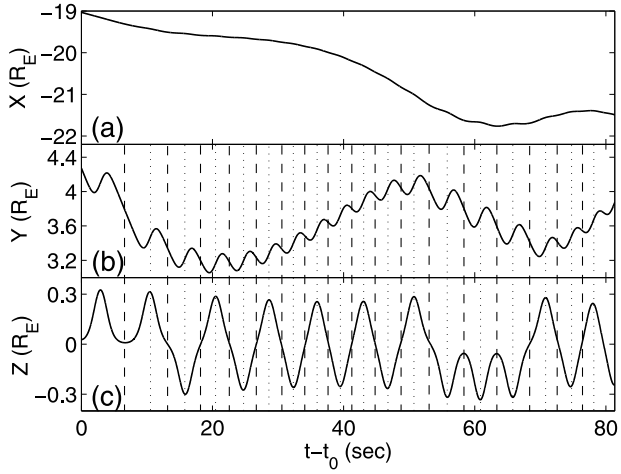

Figure 4. The trajectory of a typical warmer ion staying within the modeled thin current sheet for 81 s after the onset time (t_0) of magnetic reconnection: (a) x, (b) y, and (c) z locations of the ion as functions of time. The dashed and dotted vertical lines indicate the times at which the ion is near the neutral sheet and the times it is located at the edge of the current sheet, which also correspond to the dawnward and duskward ion motions, respectively.

type trajectories [*Speiser*, 1965] in the presence of a small southward magnetic field, which could be essentially treated as the meandering orbits superposed with the slower gyrating orbits around the southward B_z. Besides the acceleration caused by the dawn-dusk electric field, most of the duskward moving ions, according to *Speiser* [1965], would turn tailward during their gyrating motions around B_z before they are eventually ejected from the current sheet within their half-gyroperiod, which is ~16 s, for a $|B_z|$ = 2.0 nT.

[19] As the magnetic field remains southward for a much longer time than the ion half-gyroperiod, during 0451:47–0451:56 UT, most of the initially duskward meandering ions are expected to have been ejected from the current sheet, which agrees with the observed reduction of the warmer ions shown in Figures 1e and 1f. The reduction can be also clearly seen in the simulation result, shown in Figures 3e and 3f as the yz and xy cuts of the simulated ion distribution.

[20] It is interesting to note that the warmer ion component does not fully vanish during this time interval. Instead, the observations and the simulations both suggest that there exists a less populated warmer ion component streaming duskward and tailward, which is well separated from the colder component. The persistence of the warmer ion component suggests that some of the ions stay within the current sheet much longer than their half-gyroperiod around B_z. To understand the motions of these ions, a typical ion trajectory obtained in the simulation is shown in Figure 4, with the ion reaching the spacecraft location at 0451:51 UT at the velocity of 250 km/s in the tailward direction and 1150 km/s in the duskward direction, shown as the red star in Figure 3f. Figures 4a–4c show the time-dependent x, y, and z locations of the typical ion trajectory, respectively. Here the x and y locations are the GSM locations, while the z position is slightly shifted with z = 0 corresponding to the location of the neutral sheet in the modeled equilibrium.

[21] As is shown in Figure 4a, the ion is moving mainly in the tailward direction, which can be understood by the dawn-dusk electric field adopted in the model. As suggested before, the E_y field plays the role of adding a convection velocity of $v_c(x, t) = E_y(x, t)/B_z(x, t)$ in the x direction, which could be treated as the local deHoffman-Teller velocity in which E_y vanishes. The ion therefore behaves to some extent like pickup particles [e.g., *Drake et al.*, 2009] as the reconnection-associated E_y and B_z fields appear in the current sheet. Taking the typical values of $B_z = -2.0$ nT and $E_y = 0.36$ mV/m, the convection velocity equals 180 km/s in the tailward direction, which agrees with the simulated x motion shown in Figure 4a.

[22] Besides the tailward motion, the ion also oscillates in the z direction with the period less than 10 s and in the y direction with the period of ~50 s, shown in Figures 4c and 4b, respectively. The ion trajectory is shown to switch back and forth between the neutral sheet-crossing and the noncrossing segments, which is a key feature of cucumber-type trajectories [*Büchner and Zelenyi*, 1989]. The noncrossing segments (with the $t - t_0$ values in the ranges of ~0–15 and ~55–70 seconds) appear only when the overall motion of the ion is in the dawnward direction, which also agrees with the cucumber-type trajectory features.

[23] Therefore the ion trajectory is essentially the cucumber-type trajectory in the local deHoffman-Teller frame, which covers up the x oscillations associated with the cucumber-type orbit at the same period of the y oscillations (~50 s). It is thus suggested that some of the initially meandering ions may remain trapped by following cucumber-type trajectories within the current sheet after reconnection and a separated peak in the velocity space may be gradually generated by these cucumber-type trajectories that are thereby remotely sensing the presence of an X-type geometry.

[24] Another interesting feature of the ions following cucumber-type trajectories is that they move duskward when they are located at the edge of the current sheet (marked in Figures 4b and 4c as the dotted vertical lines) contributing positively to the cross-tail current, and move dawnward near the neutral sheet (marked as the dashed lines) with negative contributions. Their integrated contribution to the cross-tail current, however, is zero because of their circular motions in the xy plane. In the initial TCS equilibrium, on the other hand, a significant portion of the cross-tail current is carried by meandering ions [*Zhou et al.*, 2009]. Therefore the cross-tail current would be reduced as reconnection happens and the meandering ions start to follow cucumber-type trajectories, which might ultimately destroy the TCS structure.

4. Discussions

[25] Figure 5 suggests the ion distribution observed during 0451:02–0451:29 UT by the THEMIS probe P2 (TH-C), which was farther away from the neutral sheet than P1, as evidenced by the enhanced magnetic field [see *Angelopoulos et al.*, 2008, Figure 3G] and was located earthward of the reconnection site [*Angelopoulos et al.*, 2008]. Note that the resolution was lower as P2 was not in burst mode, and we averaged the ion distribution over a longer time (9 spin periods) to minimize the statistical fluctuations.

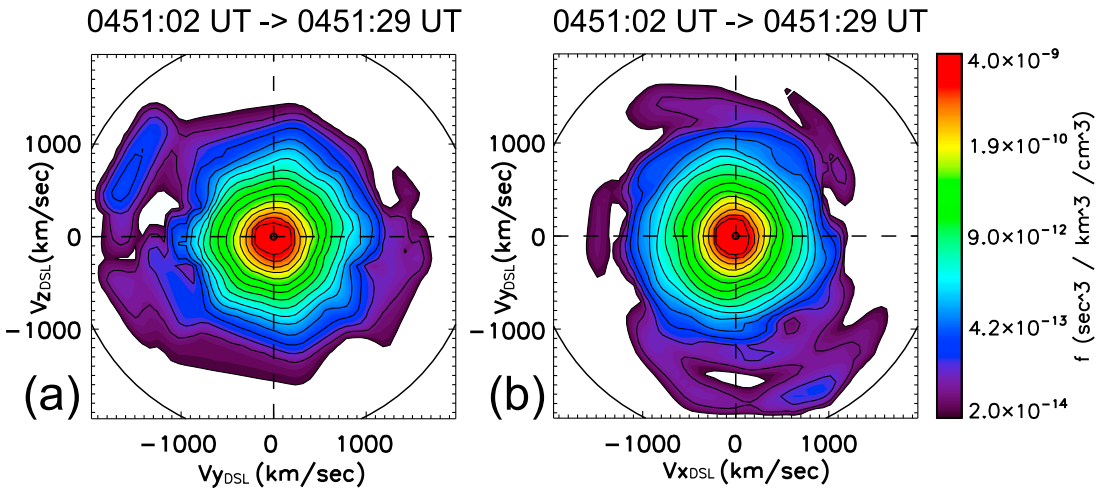

Figure 5. The (a) *yz* and (b) *xy* cuts of the ion distribution function observed by THEMIS P2 during 0451:02–0451:29 UT in despun spacecraft coordinates.

[26] Similar to the P1 observations shown in Figures 1e and 1f, the ion distribution observed by P2 also suggests a phase space density peak well separated from the isotropic colder ions that dominate the density moment, although there are differences between the P1 and P2 observations as well. For instance, the phase space densities of the P2 peak ions are much lower, barely exceeding the background noise levels, which could be understood by the greater distance of P2 from the neutral sheet (see *Zhou et al.* [2009, Figure 5b], suggesting a lower percentage of the warmer ion density in the TCS equilibrium for a greater distance to the neutral sheet). More interestingly, the P2 peak is in the duskward and earthward directions instead of the duskward and tailward directions of the P1 case, which agrees with the fact that P2 was located earthward (rather than tailward of the P1 case) of the reconnection site remotely sensing the X-type geometry.

[27] The diagnostic signatures of magnetic reconnection observed by P1 and P2 therefore could help determine the reconnection onset time, which is the key to resolving the controversies regarding whether substorm phenomena are triggered by tail reconnection at ~20 R_E or by current disruption at ~10 R_E. In this particular substorm event, *Lui* [2009] challenged the conclusions drawn by *Angelopoulos et al.* [2008] that the substorm was triggered by tail reconnection. It was argued that the conventional signatures of magnetic reconnection, namely, the tailward plasma flow with southward B_z, were observed after 0453 UT, later than the process of near-Earth current disruption.

[28] As was pointed out by *Angelopoulos et al.* [2009], the "conventional" signatures of magnetic reconnection were expected only if the observations were made near the neutral sheet, which was not the case as P1 and P2 were both located outside the neutral sheet. Therefore reconnection could only be identified on the basis of signatures expected outside the neutral sheet. In addition to the evidence shown by *Angelopoulos et al.* [2008, 2009], our results, that magnetic reconnection and X-type geometry could be remotely sensed tailward/earthward of the reconnection site by the separated phase space density peak in the duskward and tailward/earthward directions, further substantiate the conclusion that the reconnection occurred at ~0450:30 UT, well before substorm expansion onset.

5. Summary

[29] Key features of the ion distributions observed in the thin current sheet tailward of the magnetic reconnection site have been studied during the 26 February 2008 substorm event, with a separated peak of ion phase space densities gradually appearing in the tailward and duskward direction. Test particle simulations have been performed to reproduce and to understand these features, which suggest that the separated peak in the velocity space is generated by those ions following cucumber-type trajectories in a magnetic field with an X-type geometry. The similarities between simulations and observations therefore not only provide the first observational evidence (to the authors' knowledge) of the existence of the cucumber-type trajectories in the tail current sheet but also act as diagnostic signatures of reconnection for studying the time history of events during substorms.

[30] **Acknowledgments.** The work was supported by NASA grant NAS5-02099. The authors thank V. A. Sergeev, P. Pritchett, and S. S. Li for valuable discussions.

[31] Wolfgang Baumjohann thanks James Drake and Victor Sergeev for their assistance in evaluating this paper.

References

Angelopoulos, V. (2008), The THEMIS Mission, *Space Sci. Rev.*, *141*, 5–34, doi:10.1007/s11214-008-9336-1.

Angelopoulos, V., et al. (2008), Tail reconnection triggering substorm onset, *Science*, *321*, 931–935, doi:10.1126/science.1160495.

Angelopoulos, V., et al. (2009), Response to comment on "Tail reconnection triggering substorm onset," *Science*, *324*, 1391, doi:10.1126/science.1168045.

Asano, Y., T. Mukai, M. Hoshino, Y. Saito, H. Hayakawa, and T. Nagai (2004), Statistical study of thin current sheet evolution around substorm onset, *J. Geophys. Res.*, *109*, A05213, doi:10.1029/2004JA010413.

Ashour-Abdalla, M., J. P. Berchem, J. Buechner, and L. M. Zelenyi (1993), Shaping of the magnetotail from the mantle: Global and local structuring, *J. Geophys. Res.*, *98*, 5651–5676, doi:10.1029/92JA01662.

Auster, H. U., et al. (2008), The THEMIS fluxgate magnetometer, *Space Sci. Rev.*, *141*, 235–264, doi:10.1007/s11214-008-9365-9.

Baumjohann, W., et al. (2007), Dynamics of thin current sheets: Cluster observations, *Ann. Geophys.*, *25*, 1365–1389.

Bonnell, J. W., F. S. Mozer, G. T. Delory, A. J. Hull, R. E. Ergun, C. M. Cully, V. Angelopoulos, and P. R. Harvey (2008), The Electric Field Instrument (EFI) for THEMIS, *Space Sci. Rev.*, *141*, 303–341, doi:10.1007/s11214-008-9469-2.

Büchner, J., and J.-P. Kuska (1998), Consequences of strong ion acceleration in current sheets and due to reconnection, *Adv. Space Res.*, *21*, 567–572, doi:10.1016/S0273-1177(97)00965-4.

Büchner, J., and L. M. Zelenyi (1989), Regular and chaotic charged particle motion in magnetotaillike field reversals: 1. Basic theory of trapped motion, *J. Geophys. Res.*, *94*, 11,821–11,842.

Drake, J. F., M. Swisdak, T. D. Phan, P. A. Cassak, M. A. Shay, S. T. Lepri, R. P. Lin, E. Quataert, and T. H. Zurbuchen (2009), Ion heating resulting from pickup in magnetic reconnection exhausts, *J. Geophys. Res.*, *114*, A05111, doi:10.1029/2008JA013701.

Hoshino, M., T. Mukai, T. Yamamoto, and S. Kokubun (1998), Ion dynamics in magnetic reconnection: Comparison between numerical simulation and Geotail observations, *J. Geophys. Res.*, *103*, 4509–4530, doi:10.1029/97JA01785.

Lottermoser, R.-F., M. Scholer, and A. P. Matthews (1998), Ion kinetic effects in magnetic reconnection: Hybrid simulations, *J. Geophys. Res.*, *103*, 4547–4560, doi:10.1029/97JA01872.

Lui, A. T. Y. (2009), Comment on "Tail reconnection triggering substorm onset", *Science*, *324*, 1391, doi:10.1126/science.1167726.

Martin, R. F., Jr., and T. W. Speiser (1988), A predicted energetic ion signature of a neutral line in the geomagnetic tail, *J. Geophys. Res.*, *93*, 11,521–11,526, doi:10.1029/JA093iA10p11521.

McFadden, J. P., C. W. Carlson, D. Larson, M. Ludlam, R. Abiad, B. Elliott, P. Turin, M. Marckwordt, and V. Angelopoulos (2008), The THEMIS ESA plasma instrument and in-flight calibration, *Space Sci. Rev.*, *141*, 277–302, doi:10.1007/s11214-008-9440-2.

Nakamura, M. S., M. Fujimoto, and K. Maezawa (1998), Ion dynamics and resultant velocity space distributions in the course of magnetotail reconnection, *J. Geophys. Res.*, *103*, 4531–4546, doi:10.1029/97JA01843.

Pu, Z. Y., et al. (2009), THEMIS observations of magnetotail reconnection-initiated substorms on February 26, 2008, *J. Geophys. Res.*, doi:10.1029/2009JA014217, in press.

Runov, A., et al. (2008), Observations of an active thin current sheet, *J. Geophys. Res.*, *113*, A07S27, doi:10.1029/2007JA012685.

Schwartz, S. J., P. W. Daly, and A. N. Fazakerley (1998), Multi-spacecraft aalysis of plasma kinetics, in *Analysis Methods for Multi Spacecraft Data*, edited by G. Paschmann and P. W. Daly, pp. 159–184, Eur. Space Agency, Bern, Switzerland.

Sergeev, V. A., D. G. Mitchell, C. T. Russell, and D. J. Williams (1993), Structure of the tail plasma/current sheet at 11 Re and its changes in the course of a substorm, *J. Geophys. Res.*, *98*, 17,345–17,366, doi:10.1029/93JA01151.

Sitnov, M. I., P. N. Guzdar, and M. Swisdak (2003), A model of the bifurcated current sheet, *Geophys. Res. Lett.*, *30*(13), 1712, doi:10.1029/2003GL017218.

Sitnov, M. I., M. Swisdak, J. F. Drake, P. N. Guzdar, and B. N. Rogers (2004), A model of the bifurcated current sheet: 2. Flapping motions, *Geophys. Res. Lett.*, *31*, L09805, doi:10.1029/2004GL019473.

Sitnov, M. I., M. Swisdak, P. N. Guzdar, and A. Runov (2006), Structure and dynamics of a new class of thin current sheets, *J. Geophys. Res.*, *111*, A08204, doi:10.1029/2005JA011517.

Sonnerup, B. U. O. (1971), Adiabatic particle orbits in a magnetic null sheet, *J. Geophys. Res.*, *76*, 8211–8222.

Speiser, T. W. (1965), Particle trajectories in model current sheet: 1. Analytic solution, *J. Geophys. Res.*, *70*, 4219–4226.

Speiser, T. W., and R. F. Martin Jr. (1992), Energetic ions as remote probes of X type neutral lines in the geomagnetic tail, *J. Geophys. Res.*, *97*, 10,775–10,785, doi:10.1029/92JA00316.

Zhou, X.-Z., Z. Y. Pu, Q.-G. Zong, and L. Xie (2007), Energy filter effect for solar wind particle entry to the plasma sheet via flank regions during southward interplanetary magnetic field, *J. Geophys. Res.*, *112*, A06233, doi:10.1029/2006JA012180.

Zhou, X.-Z., et al. (2009), Thin current sheet in the substorm late growth phase: Modeling of THEMIS observations, *J. Geophys. Res.*, *114*, A03223, doi:10.1029/2008JA013777.

V. Angelopoulos, A. Runov, and X.-Z. Zhou, Institute of Geophysics and Planetary Physics, University of California, Los Angeles, CA 90065-1567, USA. (xzhou@igpp.ucla.edu)

Z. Y. Pu and Q.-G. Zong, School of Earth and Space Sciences, Peking University, Beijing 100871, China.

M. I. Sitnov, Johns Hopkins University Applied Physics Laboratory, 11100 Johns Hopkins Road, Laurel, MD 20723-6099, USA.